Title

Bioelectronic light-gated transistors with biologically tunable performance.

Permalink

https://escholarship.org/uc/item/6w3405z7

Journal

Advanced materials (Deerfield Beach, Fla.), 27(5)

ISSN

0935-9648

Authors

Tunuguntla, Ramya H
Bangar, Mangesh A
Kim, Kyunghoon
et al.

Publication Date

2015-02-01

DOI

10.1002/adma.201403988

Peer reviewed

Bioelectronic Light-Gated Transistors with Biologically Tunable Performance

Ramya H. Tunuguntla, Mangesh A. Bangar, Kyunghoon Kim, Pieter Stroeve, Costas Grigoropoulos, Caroline M. Ajo-Franklin, and Aleksandr Noy*

Biological systems interact with their environments by controlling proton and ion gradients, and membrane electric potentials to accomplish strikingly complex tasks on the nanometer length scale. Energy harvesting, motility, and whole organism replication involves a vast arsenal of active and passive ion channels, and ion pumps that mediate complex and precise transport across biological membranes.[1] Despite the remarkable rate of progress exhibited by modern microelectronic devices, they still cannot compete with the ability of biological molecules to carry out molecular recognition, catalyze chemical reactions, and respond and adapt to environmental cues. Therefore, the sophistication of biomolecules provides an excellent opportunity to use them in hybrid bioelectronic devices where such a combination could enhance electronic functionality and create seamless bidirectional interfaces between man-made and biological structures.[2]

1D inorganic nanostructures, which have critical dimensions comparable to the sizes of biological molecules, form a versatile materials platform for building such integrated assemblies. Researchers already use silicon nanowire (SiNW) field-effect transistors (FETs) functionalized with molecular recognition sites in biosensing,[3,4] nucleic acid detection,[3] drug development applications,[5] neuronal activity monitoring,[6] and cyborg tissue scaffolds.[7] However, most of these applications utilize molecular recognition as a biosensing mechanism, or use the devices as direct sensors for electrochemical potential. In contrast, major biological signaling processes, such as neural signaling often rely on a much more intricate interplay between ion gradients and membrane potentials.

Here, we demonstrate the use of a similar biological regulation mechanism in a light-powered bioelectronic device based on a 1D lipid bilayer device architecture. In these devices, a membrane protein resides within the lipid bilayer that covers a nanowire channel of a SiNW FET. This lipid bilayer performs two functions: it shields the nanowire from the solution species and serves as a native-like environment for membrane proteins that preserves their functionality, integrity, and vectorality. In the past, we showed that this architecture allows us to couple passive ion transport[8] and active ATP-driven ion transport to the electronic signaling.[9] In this work, we achieve two goals. We show a 1D bilayer device incorporating a bacteriorhodopsin (bR) proton pump that couples light-driven proton transport to a bioelectronic circuit output. We also show that coassembly of protein channels and ionophores in the 1D bilayer device can upregulate and downregulate its output level by altering the lipid membrane permeability to specific ions, which in turn modulates the membrane potential.

Our device platform (**Figure 1**a) was based on a microfabricated SiNW FET in which a single nanowire was clamped between a pair of source and drain electrodes insulated from the solution by a protective photoresist layer. All devices measured in this study were single nanowire devices similar to the device in Figure S2 (Supporting Information). A microfluidic channel filled with a buffer solution covered the active area of the chip. This configuration allowed us to fuse proteoliposomes onto the SiNW surface to create a continuous lipid bilayer that preserved the protein functionality. The lipid bilayer covering the nanowire surface contained bR, a protein from the purple membrane of *Halobacterium salinarum*. bR absorbs green light (λ_{max} = 560 nm) and undergoes a multistate photocycle that translocates a proton across the membrane.[10] In bacteria, this process builds up the proton motive force that subsequently powers ATP synthesis.[11] bR is also exceptionally stable ex vivo under diverse environmental stresses, and over a broad range of pH and temperature.[12] In this study, our devices were tested over 3–4 days without any loss of signal. It is possible that the overall device stability could be compromised over a longer timescale in physiological conditions,[13] however it is not clear how lipid bilayer coating would affect this process.

Dr. R. H. Tunuguntla, Dr. M. A. Bangar,
Dr. K. Kim, Prof. A. Noy
Biology and Biotechnology Division
Physical and Life Sciences Directorate
Lawrence Livermore National Laboratory
Livermore, California 94550, USA
E-mail: noy1@llnl.gov
Dr. R. H. Tunuguntla, Prof. P. Stroeve
Materials Science and Chemical Engineering Department
University of California Davis
Davis, California 95616, USA
Dr. R. H. Tunuguntla, Dr. M. A. Bangar, Dr. K. Kim,
Dr. C. M. Ajo-Franklin, A. Noy
The Molecular Foundry
Materials Sciences Division
Dr. K. Kim, Prof. C. Grigoropoulos
Mechanical Engineering Department
University of California Berkeley
Berkeley, California 94704, USA
Dr. C. M. Ajo-Franklin
Physical Biosciences Division
Lawrence Berkeley National Laboratory
Berkeley, California 94720, USA
Prof. A. Noy
School of Natural Sciences
University of California Merced
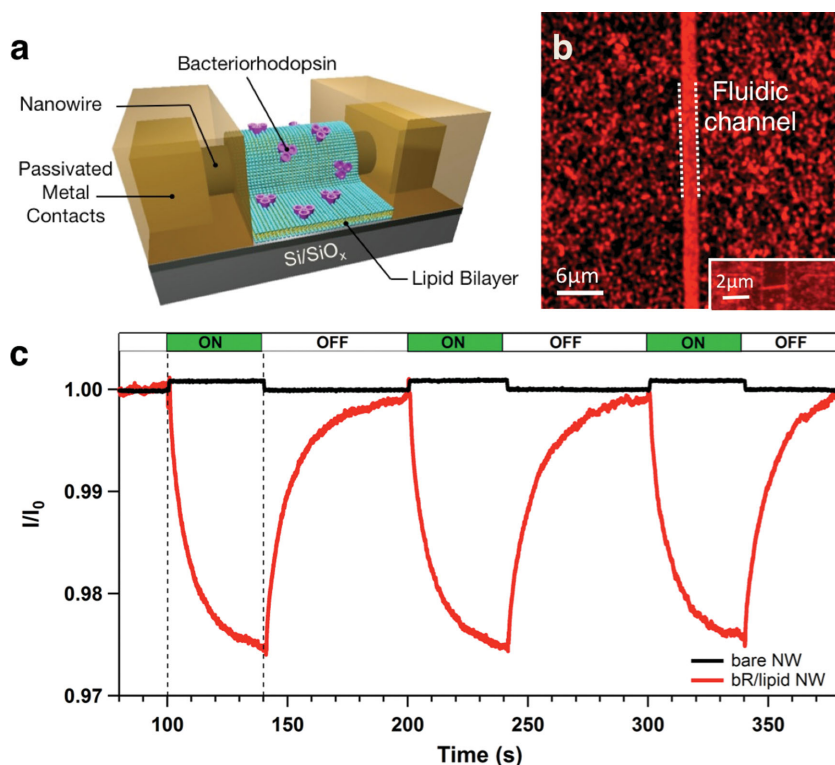Merced, California 95340, USA

Figure 1. Light-activated bioelectronic device. a) Device schematics showing a SiNW transistor with the nanowire covered with a lipid bilayer containing bacteriorhodopsin protein. b) Scanning confocal microscopy image of the chip coated with lipid bilayer. To visualize the bilayer a small portion of the lipid was labeled with a TexasRed™ fluorescent dye. Inset: a scanning confocal microscope image of a source and a drain electrode region of the chip showing a SiNW covered with lipid bilayer. c) Normalized time trace of the SiNW transistor source–drain current recorded under three cycles of green light (560nm) illumination for the uncoated SiNW device (black trace) and the device coated with a lipid bilayer containing bR protein (red trace). Data representative of 21 devices.

After we reconstituted bR into preformed 1,2-dioleoyl-sn-glycero-3-phosphocholine (DOPC) liposomes and fused the resulting proteoliposomes onto the device surface, fluorescence microscopy images (Figure 1b) indicated that the lipid bilayer covered the nanowire device completely. Moreover, fluorescence recovery after photobleaching measurements indicated that the lipid bilayer covering the nanowire was continuous and mobile (Figure S3, Supporting Information); both of these properties are important for providing good shielding of the SiNW surface and accommodating the membrane proteins.

Upon exposure to 560 nm green light, the SiNW devices that did not contain membrane protein registered only small amounts of photocurrent (Figure 1c, black trace).[14] This signal was quite small (the maximum conductance change was less than 0.1%) and exhibited almost instantaneous turn-on and turn-off kinetics: upon illumination the signal immediately increased to a steady-state level, which then decayed back to baseline level as soon as the light was turned off. When the lipid membrane covering the SiNW contained bR protein, the device showed a markedly different response to the green light exposure (Figure 1c, red trace). Unlike the photocurrent signal, the source–drain current showed a fast initial decrease that gradually slowed down. The resulting signal exceeded the

photocurrent by at least an order of magnitude. After the illumination was switched off, the current gradually returned to its original level. This cycle was repeatable (Figure 1c) without significant losses of signal strength or fidelity.

A quantitative description of ion fluxes in this device accounts for the interplay of the two major processes. Upon exposure to green light, the bR proteins in the lipid membrane pump protons across the bilayer and build up a proton gradient across the barrier. The resulting change in the SiNW surface charge due to the protonation of SiO⁻ groups causes a change in the transistor output.[15] Simultaneously, passive diffusion of protons across the lipid bilayer tries to equilibrate the proton concentration on both sides of the membrane and reduces the device response. Both of these processes also modify the electrochemical potential across the membrane, which is set by a combination of the pump activity and the passive diffusion of all ionic species present in the system through the membrane. Qualitatively, as the proton gradient increases, the rate of proton leakage goes up. At the same time, the proton pumping rate is retarded by the electrochemical gradient built up on the membrane.[16] As the pumping and leakage processes offset each other, the device output current slows down and eventually reaches a steady state. When the light is switched off and bR stops pumping protons, the leakage through the bilayer continues to deplete the transmembrane proton gradient and eventually returns the device to its baseline state, where it becomes ready for the next illumination cycle. The device response was then converted into the proton concentration in the solution between the nanowire and the bilayer using a calibration curve (Figure S5, Supporting Information) measured for each batch of the devices used in this study. The remaining data presented in this study are reported in terms of proton concentration change.

The main differential equation describing the proton gradient buildup accounts for the contributions of pumping and leakage processes:

$$\frac{dH(t)}{dt} = I_0(V_m)\frac{A}{v} - P_H(H(t) - H_0)\frac{A}{v} \tag{1}$$

where $H(t)$ is the proton concentration between the bilayer and the nanowire surface, H_0 is the proton concentration of the outside solution, V_m is the electrochemical potential of the membrane, $I_0(V_m)$ is the protein pumping rate, which is a function of the membrane potential and incident light intensity, P_H is the proton permeability of the lipid bilayer, and $\frac{A}{v}$ is the surface-to-volume ratio for the solution enclosed between the bilayer and the nanowire. The membrane potential can be

determined from the concentrations and permeabilities of the ions present in the system in the inner and outer solutions using Goldman–Hodgkin–Katz (GHK) equation:

$$V_m = -\frac{RT}{F}\ln\frac{P_H H_{in} + P_K K_{in} + P_{Cl} C_{out}}{P_H H_{out} + P_K K_{out} + P_{Cl} C_{in}} \qquad (2)$$

where P_i is the membrane permeability of ion of type i; subscripts H, K, and Cl denote the concentrations of proton, potassium, and chloride ions, and subscripts in and out denote concentrations on inner and outer sides of the membrane. R, T, and F are the ideal gas constant, temperature, and Faraday's constant. Finally, we assume that the membrane potential retards the activity of the bR pump linearly[17] up to a point when it reaches the stalling value, V_{max}. Then the main differential equation governing the proton gradient buildup becomes:

$$\frac{dH(t)}{dt} = \frac{I_0 A}{v}\frac{V_{max} - V_m}{V_{max}} - \frac{P_H A}{v}(H(t) - H_0) \qquad (3)$$

where the value of the membrane potential of V_m is set by the GHK equation (Equation 2). After the illumination is turned off ($I_0 = 0$), the leakage of the protons is described by:

$$\frac{dH(t)}{dt} = -\frac{P_H A}{v}(H(t) - H_0) \qquad (4)$$

It follows immediately from the Equation 4 that the time constant for the leakage process, τ, should be equal to $\frac{v}{A \times P_H}$. Since most of the measured leakage time constant values cluster around the value of 10 s (**Figure 2**a, inset), then using the proton permeability value[18] of 5.9×10^{-9} m s^{-1} we can estimate the surface-to-volume ratio, $\frac{A}{v}$, as 1.69×10^7 m^{-1}. The inverse of this value, 60 nm, which corresponds to the effective thickness of the proton reservoir between the nanowire and the lipid bilayer overhang dimension, gives us important information about the geometry of the device. This value is much larger than ca. 2 nm value for the distance between the nanowire and the lipid bilayer that coats it conformally (Figure 2a). Instead, this value is comparable to the size of the nanowire, giving strong evidence that the majority of the protons delivered by the pump accumulate in the "pocket" space formed on the sides of nanowire (Figure 2a). This observation explains the variations in the leakage time measured in different devices, which likely reflect the differences in the nanowire sizes and the corresponding variations in the surface-to-volume ratio. We note that overhanging portion of the bilayer with this geometry should still remain robust.[19] Finally, these observations suggest a straightforward pathway toward increasing the recovery speed of the device by implementing a suspended nanowire configuration, which should eliminate the reservoir space altogether.

When we fit the Equation 2–4 to the kinetics of proton accumulation and dissipation (Figure 2a), we used the literature values for the mobilities of proton, potassium, and chloride ions ($P_K = 3.3 \times 10^{-15}$ m s^{-1}[20] and $P_{Cl} = 1.5 \times 10^{-13}$ m s^{-1}[21] and the bR stalling potential of 225 mV[17] leaving us with only one fitting parameter: the bR proton pumping rate, I_0. Even then, the kinetics predicted by the model fits the observed device response quite well (Figure 2a, dashed lines). The
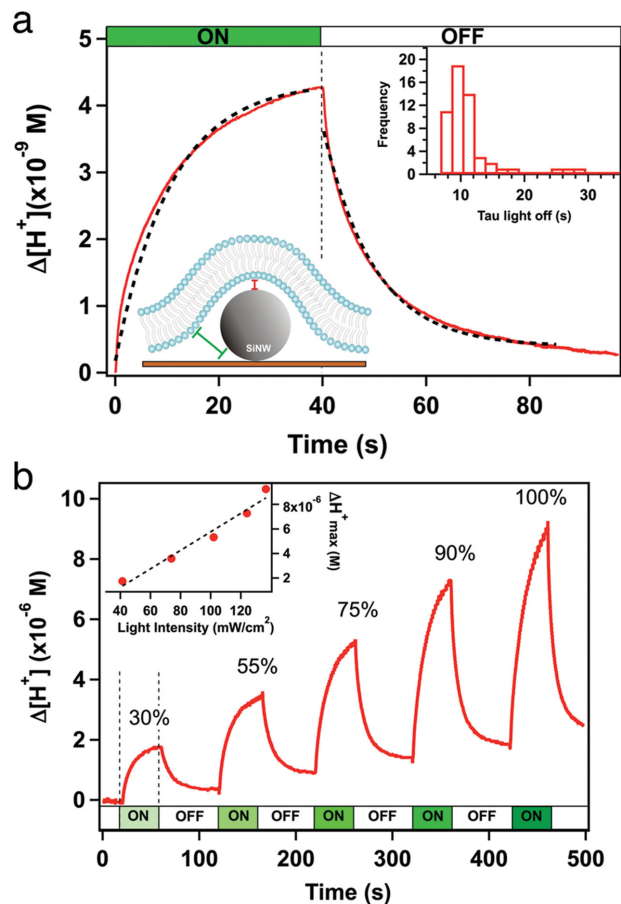

Figure 2. Kinetics of the device response. a) Time trace of the proton concentration gradient accumulated in the device over one light ON/light OFF cycle for the device incorporating bR proteins (each cycle consisted of 40 s light exposure followed by 60 s of dark time). The dashed lines represent the best fit to Equation 2 and 3. The schematic shows the device geometry with a solution reservoir on each side (the red line represents ca. 2 nm water layer between the top wire and bilayer, and the green line represents ca. 60 nm solution "pocket"). Inset: A histogram of the average proton leakage time values in the OFF state ($n = 54$). b) Time trace of changes in proton concentration on the nanowire side of the membrane under varying illumination power (data are representative of at least 18 bR-FET device measurements). Inset: A plot of the proton gradient accumulated after 40 s of illumination as a function of incident light intensity.

value of the bR pumping rate that we obtained from fitting the experimental data (2.4×10^{-3} H$^+$ s^{-1}) is about an order of magnitude lower than the values reported in the literature (2×10^{-2} H$^+$ s^{-1}).[22] We note, however, that our estimate represents a lower boundary value, because it assumes that every bR protein in the lipid bilayer incorporated into the device remains photoactive and that no protein amount was lost during the sample preparation steps.

A quick analysis of the terms in the Equation 2 also shows that the chloride ion terms make the largest contribution to the membrane potential. Thus, since the chloride ion concentration is many orders of magnitude larger than the proton concentration change, we can conclude that the electrochemical potential variations are relatively small. Thus, the device current saturates

when the proton leakage rate balances the pump rate. We can estimate that at this point the membrane potential reaches only 18 mV, which is well below the bR stalling potential. Finally, the model predicts that the initial pumping rate should show the linear dependence on the intensity of the incident light, at least until bR activity reaches saturation. Indeed, the values of the initial pumping rates that we measured at five different light intensities follow this linear dependence (Figure 2b).

The dynamic equilibrium between the pumping and leakage processes and the membrane potential also gives us an opportunity to regulate the device performance using ionophore species that modulate the membrane potential by changing the membrane permeability to the specific ions. Three different ionophores that self-insert into the bilayer allowed us to vary different components of the proton electrochemical gradient independently. Qualitatively, valinomycin, a hydrophobic carrier molecule that shuttles K^+ ions across the membrane,[20] relieves the electric field gradient across the membrane but leaves the proton gradient intact. Nigericin, a transmembrane carrier that catalyzes an electroneutral K^+/H^+ exchange across the lipid bilayer,[23] relieves the proton gradient, but preserves the electric field gradient. Finally, gramicidin A (gramA), a peptide that forms a passive channel in the membrane, allows fast nonspecific ion leakage[24] and neutralizes both of these gradients.

Valinomycin, which helps K^+ ions to cross the membrane (increasing the effective K^+ membrane permeability by two orders of magnitude to a value of 5.0×10^{-13} m s^{-1}), provides an additional compensatory pathway to relieve the electrical potential across the bilayer while keeping the proton gradient intact. Thus, it should upregulate the device performance. Indeed, addition of 2 µM of valinomycin to the 1D bilayer device increased the peak proton accumulation under the bilayer surface by ca. 50% (decreasing the pH by an additional 0.3 units) compared with devices containing only bR (**Figure 3**a). This effect was also repeatable over multiple light ON/OFF cycles. Significantly, the kinetic curve of the
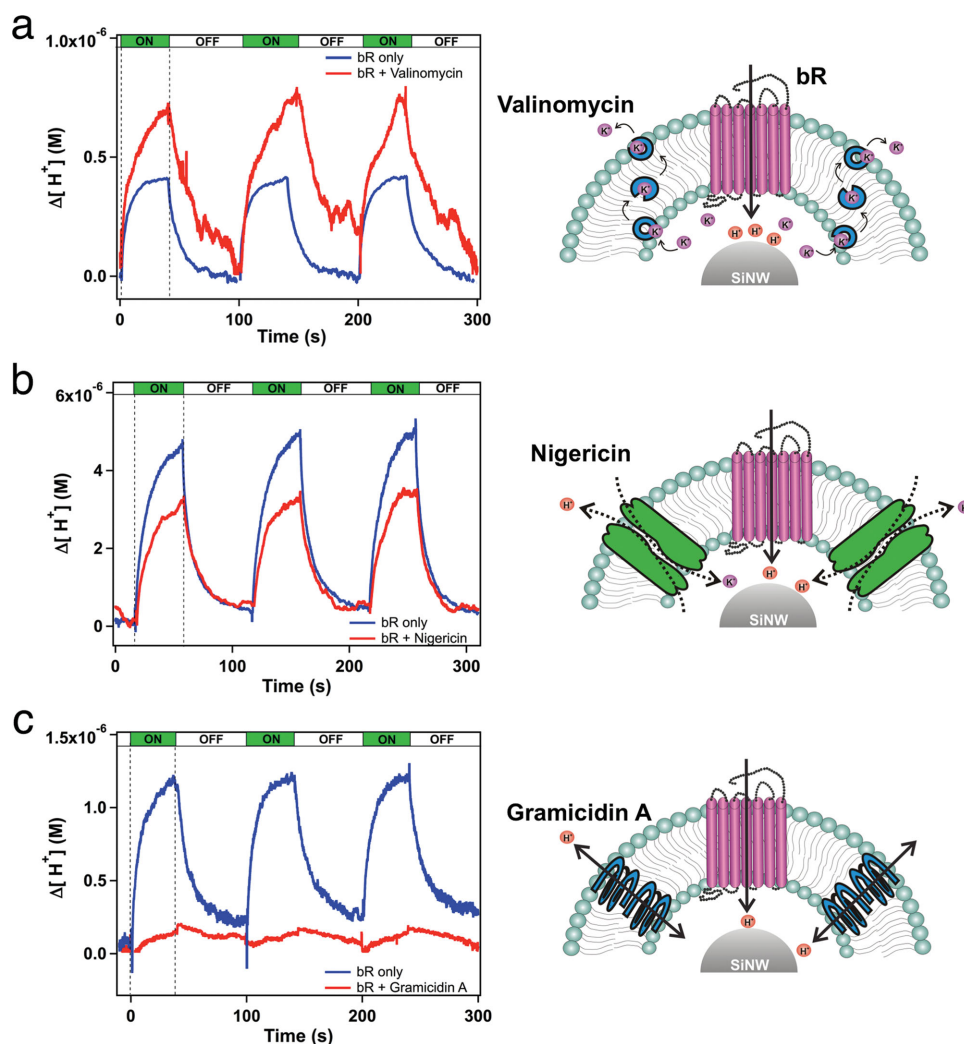

Figure 3. Device response in presence of ionophores shown as time traces of the proton concentration under the lipid bilayer in the vicinity of the SiNW during three consecutive 40 s illumination cycles for the devices incorporating bR protein and a) valinomycin, b) nigericin, and c) gramicidin A. Schematics on the right illustrate the action mechanism for each ionophore. (Data representative of at least seven bR-FET device measurements for each ionophore).
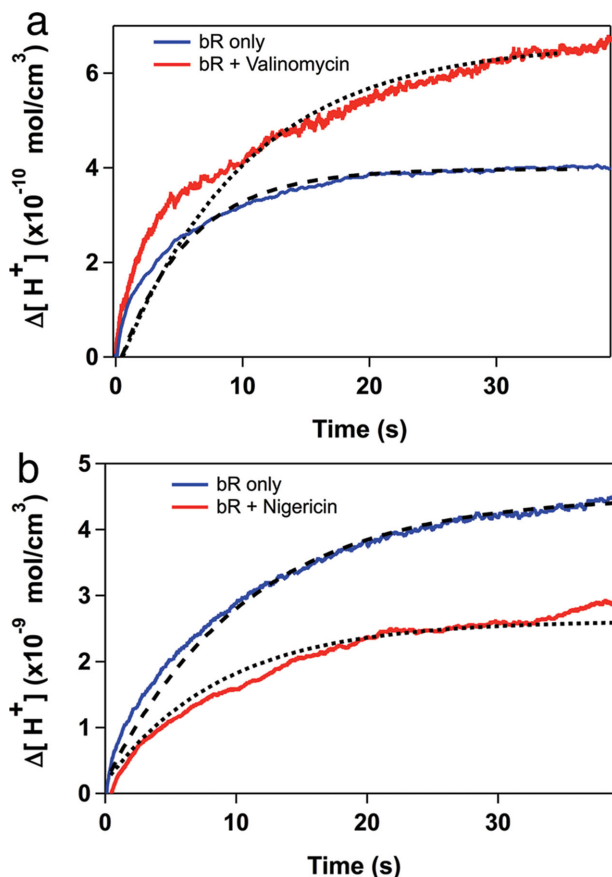
Figure 4. Changes in membrane permeability modulate device output. a) A comparison of the measured device outputs during the illumination period before (blue curve) and after (red curve) addition of 2 μM valinomycin ionophore to enhance potassium permeability and the kinetic curves calculated using Equation 2–4 (dashed curve, $P_K = 3.3 \times 10^{-15}$ m s^{-1}; dotted curve, $P_K = 5.0 \times 10^{-13}$ m s^{-1}). b) A comparison of the measured device output during the illumination period before (blue curve) and after (red curve) addition of 2 μM nigericin ionophore that creates an additional pathway for proton leakage and the kinetic curves calculated using Equation 2–4 (dashed curve, $P_H = 5.9 \times 10^{-9}$ m s^{-1}; dotted curve, $P_H = 7.0 \times 10^{-9}$ m s^{-1}). See the main text for the description of parameters used for the calculation in each case.

proton accumulation calculated using Equation 2–4 with only an increased potassium ion permeability (every other model parameter remained unchanged) reproduced the measured increase in the device output (**Figure** 4a).

Nigericin facilitates the backflux of the protons pumped under the bilayer by bR, thus providing an additional relief pathway for the proton gradient. Since this action is accompanied by the coupled flux of potassium ions in the opposite direction, this ionophore preserves the electrical field gradient developed by bR. By providing an extra leakage pathway for the protons, nigericin effectively increases the permeability of protons through the lipid bilayer; therefore, the maximum signal achieved by the device should also be reduced relative to the signal obtained before introduction of the ionophore. Indeed, the experiment shows (Figure 3b) that after addition of 2 μM of nigericin the maximum proton accumulation decreased by ca.

35% (a ΔpH difference of 0.2 units) compared with the devices with only the bR protein. In this instance, we also found that we could reproduce the measured kinetic curves using Equation 2–4 and adjusting again only one parameter — the proton permeability (P_H) from 5.9×10^{-9} to 7.0×10^{-9} m s^{-1} (Figure 4b). Ionophores did not modulate the device response (i.e., photocurrent) in absence of bR protein. Thus, the model represented by Equation 2–4 provides a complete quantitative description of all processes that occur in these multicomponent bioelectronic devices and highlights the membrane ion equilibrium as the main physical process that controls device output.

We also explored a way to drastically increase the proton leakage rate though the lipid bilayer by introducing gramA into our devices. Gram A is a passive pore that exhibits high permeability for protons and monovalent ions. The presence of gramA pores in the bilayer-coated device effectively shorts the lipid membrane and provides a major pathway to relieve all ion and proton gradients in the system. Indeed, when we introduced gramA to our devices, most of the proton pump activity was suppressed and we observed only very small SiNW conductance change in response to the green light illumination (Figure 3c).

In summary, we demonstrated that hierarchical assembly of membrane protein pumps and ionophore molecules created biologically tunable bioelectronic devices that converted light-induced proton transport by bR protein into an electronic signal. Our results show that ionophore molecules, coassembled with the membrane protein, upregulate and downregulate the device output by modulating the lipid membrane potential and altering the specific ion permeability of the membrane. We have also presented a quantitative model that describes the observed kinetics and regulation mechanisms with high accuracy.

These results open up new opportunities for constructing bioelectronic devices. The incorporation of a robust proton pump capable of developing significant pH gradients is a major step toward integration of other biological processes powered by proton gradients such as spreading of neutrophils, elimination of CO_2 by epithelial cells, or production of ATP by ATPase enzymes. Significantly, the possibility to tune the device performance by using biological modifiers coassembled in the membrane covering the nanowire gives researchers a much more extensive biological toolkit for bioelectronics applications such as implantable biosensors and neural interfaces.

Experimental Section

SiNW Growth and FET Device Fabrication: P-type SiNWs with diameters in the range of 40–80 nm were grown using catalytic chemical vapor deposition. SiNWs were aligned onto a SiO$_2$ surface using a flow-alignment technique.[25] The source–drain electrode contacts, with a typical spacing of 5 μm, were patterned on the wafer using photolithography, and the chip was subsequently passivated with an additional photoresist layer, creating a 2 μm channel exposing the SiNWs. These devices were then placed into a polydimethylsiloxane (PDMS) fluid cell with inlet/outlet ports for solution delivery, and an opening for a leak-free gate electrode (see details in the Supporting Information).

Proteoliposome Preparation and Characterization: DOPC proteoliposomes were prepared using the detergent-mediated reconstitution method[26] in 150 mM KCl, 1 mM KH_2PO_4, pH 6.8 at a protein:lipid molar ratio of 1:500. Successful incorporation of bR (Sigma–Aldrich) into liposomes was verified using UV–vis spectroscopy and dynamic light scattering (DLS) measurements before and after reconstitution. Proteoliposome solution was injected into a PDMS channel covering the device chip and allowed to fuse for 30 min. For measurements, the PDMS channel was filled with 150 mM KCl, 1 mM KH_2PO_4, pH 6.8 buffer solution.

Confocal Laser Scanning Microscopy: Lipid bilayer coverage and mobility on the SiNW were verified by including 0.2% (mol%) TexasRed-DHPE to the lipid composition and imaging the bilayer using scanning confocal microscopy (Zeiss LSM710 with Zen software). Further experimental details are provided in the Supporting Information.

Device Measurements: Assembled devices were mounted in a shielded probe station. Transfer characteristics (I_{S-D} vs V_G) and real time (I_{S-D} vs t) measurements were recorded with a homebuilt measurement system that used a NI-DAQ card and a Keithley 428-PROG preamplifier. To improve the signal-to-noise ratio we have applied an AC bias between the source and drain electrodes and used lock-in detection to measure the source–drain current. For device photoactivation we used an external LED light source (SCHOTT KL 2500) fitted with a green (560 nm) bandpass filter (Newport Corp.). The light source output had a power density of 136 mW cm^{-2} at 100% illumination and a spot size of 1 cm in diameter. Device measurements such as I–V curve acquisition and time trace measurements were carried out using AC source–drain bias of 200 mV (amplitude) at 5 and 100 Hz frequencies. We used a liquid Ag/AgCl gate electrode to apply a gate voltage of −500 mV, which falls in the linear regime of the transfer characteristics curve (Figure S4, Supporting Information). The entire setup was electrically grounded during all measurements and there is minimal leakage current to the gate electrode ($\approx10^{-12}$ A, Figure S4, Supporting Information). To obtain quantitative information about the proton concentration in the solution surrounding the FET, we have measured the transistor source to drain current response, I_{S-D}, in the presence of varying pH buffers in the range of 4–8.

Ionophore Incorporation: The ionophores, valinomycin and nigericin, used in this study are self-inserting into the lipid membrane as reported by previous studies.[27] Ionophores, valinomycin, and nigericin, were added to the solution in the PDMS microfluidic channel at a final concentration of 2 μM and incubated in the fluid cell for approximately 30 min to allow sufficient time for incorporation into the bR containing bilayer. Afterwards, the chamber was washed with buffer. GramA was co-reconstituted with bR during proteoliposome preparation, at a ratio of 1:200 gramA:lipid.

Supporting Information

Supporting Information is available from the Wiley Online Library or from the author.

Acknowledgements

[1] B. Alberts, D. Bray, J. Lewis, M. Raff, K. Roberts, J. D. Watson, *Molecular Biology of the Cell*, Garland Science, New York **2007**.

[2] A. Noy, *Adv. Mater.* **2011**, *23*, 799.

[3] A. Gao, N. Lu, Y. Wang, P. Dai, T. Li, X. Gao, Y. Wang, C. Fan, *Nano Lett.* **2012**, *12*, 5262.

[4] a) B. He, T. J. Morrow, C. D. Keating, *Curr. Opin. Chem. Biol.* **2008**, *12*, 522; b) S.-P. Lin, C.-Y. Pan, K.-C. Tseng, M.-C. Lin, C.-D. Chen, C.-C. Tsai, S.-H. Yu, Y.-C. Sun, T.-W. Lin, Y.-T. Chen, *Nano Today* **2009**, *4*, 235.

[5] X. Duan, Y. Li, N. K. Rajan, D. A. Routenberg, Y. Modis, M. A. Reed, *Nat. Nano.* **2012**, *7*, 401.

[6] F. Patolsky, B. P. Timko, G. Yu, Y. Fang, A. B. Greytak, G. Zheng, C. M. Lieber, *Science* **2006**, *313*, 1100.

[7] B. Tian, J. Liu, T. Dvir, L. Jin, J. H. Tsui, Q. Qing, Z. Suo, R. Langer, D. S. Kohane, C. M. Lieber, *Nat. Mater.* **2012**, *11*, 986.

[8] N. Misra, J. A. Martinez, S.-C. Huang, Y. Wang, P. Stroeve, C. Grigoropoulos, A. Noy, *Proc. Natl. Acad. Sci. USA* **2009**, *106*, 13780.

[9] S.-C. Huang, A. Artyukhin, N. Misra, J. Martinez, P. Stroeve, C. Grigoropoulos, J.-W. Ju, A. Noy, *Nano Lett.* **2010**, *10*, 1812.

[10] A. Royant, K. Edman, T. Ursby, E. Pebay-Peyroula, E. M. Landau, R. Neutze, *Nature* **2000**, *406*, 645.

[11] R. H. Lozier, R. A. Bogomolni, W. Stoeckenius, *Biophys. J.* **1975**, *15*, 955.

[12] V. Thavasi, T. Lazarova, S. Filipek, M. Kolinski, E. Querol, A. Kumar, S. Ramakrishna, E. Padrós, V. Renugopalakrishnan, *J. Nanosci. Nanotechnol.* **2009**, *9*, 1679.

[13] W. Zhou, X. Dai, T.-M. Fu, C. Xie, J. Liu, C. M. Lieber, *Nano Lett.* **2014**, *14*, 1614.

[14] K.-H. K. Kim, D. Y. Jeong, B. Min, K. Cho, H. Kim, B. M. Moon, T. Noh, J. Park, M. Suh, S. Kim, *Jpn. J. Appl. Phys.* **2006**, *45*, 4265.

[15] Y. Cui, Q. Wei, H. Park, C. M. Lieber, *Science* **2001**, *293*, 1289.

[16] M. K. Joshi, S. Bose, R. W. Hendler, *Biochemistry* **1999**, *38*, 8786.

[17] S. Geibel, È. Lörinczi, E. Bamberg, T. Friedrich, *PloS One* **2013**, *8*, e73338.

[18] D. Deamer, *J. Bioenerg. Biomembr.* **1987**, *19*, 457.

[19] Y. Roiter, M. Ornatska, A. R. Rammohan, J. Balakrishnan, D. R. Heine, S. Minko, *Nano Lett.* **2008**, *8*, 941.

[20] S. Johnson, A. Bangham, *Biochim. Biophys. Acta, Biomembr.* **1969**, *193*, 82.

[21] Y. Toyoshima, T. Thompson, *Biochemistry* **1975**, *14*, 1525.

[22] T. Kouyama, *Biophys. J.* **1987**, *51*, 839.

[23] K. J. Hellingwerf, J. C. Arents, B. J. Scholte, H. V. Westerhoff, *Biochim. Biophys. Acta, Bioenerg.* **1979**, *547*, 561.

[24] D. A. Kelkar, A. Chattopadhyay, *Biochim. Biophys. Acta, Biomembr.* **2007**, *1768*, 2011.

[25] Y. Huang, X. Duan, Q. Wei, C. M. Lieber, *Science* **2001**, *291*, 630.

[26] M. T. Paternostre, M. Roux, J. L. Rigaud, *Biochemistry* **1988**, *27*, 2668.

[27] a) M. Zagnoni, M. Sandison, P. Marius, A. Lee, H. Morgan, *Lab Chip* **2007**, *7*, 1176; b) J. Cui, C. Li, C. Wang, Y. Li, L. Zhang, L. Zhang, X. Xiu, Y. Li, N. Wei, *Int. J. Pharm.* **2010**, *399*, 31.